Applied Catalysis B: Environmental 90 (2009) 132–140

Contents lists available at ScienceDirect

Applied Catalysis B: Environmental

journal homepage: www.elsevier.com/locate/apcatb

# Effect of potassium in calcined Co–Mn–Al layered double hydroxide on the catalytic decomposition of $N_2O$

L. Obalová [a,*], K. Karásková [a], K. Jirátová [b], F. Kovanda [c]

[a] Technical University of Ostrava, 17.listopadu 15, 708 33 Ostrava, Czech Republic
[b] Institute of Chemical Process Fundamentals of the ASCR, v.v.i., Rozvojová 135, 165 02 Prague, Czech Republic
[c] Institute of Chemical Technology, Prague, Technická 5, 166 28 Prague, Czech Republic

ARTICLE INFO

*Article history:*
Received 19 September 2008
Received in revised form 6 February 2009
Accepted 3 March 2009
Available online 13 March 2009

*Keywords:*
Nitrous oxide
Catalytic decomposition
Layered double hydroxides
Mixed oxide catalysts
Potassium promoter

ABSTRACT

A series of catalysts was prepared by thermal treatment (500 °C) of the coprecipitated Co–Mn–Al layered double hydroxide (Co:Mn:Al molar ratio of 4:1:1) doped with various amount of potassium (0–3 wt%). Obtained spinel-like mixed oxides were characterized by powder X-ray diffraction, X-ray photoelectron spectroscopy, BET surface area measurements, temperature-programmed $H_2$ reduction, and temperature-programmed $CO_2$ and $NH_3$ desorption. The prepared catalysts were tested for $N_2O$ decomposition to determine the effect of K addition on the catalytic activity in the presence of $O_2$, $NO_x$ and $H_2O$. An optimum K content of ca. 0.9–1.6 wt% was found to achieve a high catalytic activity in the presence of $O_2$ and $H_2O$, while the non-modified Co–Mn–Al mixed oxide was the most active catalyst in the presence of $O_2$ and $NO_x$. The addition of potassium to the Co–Mn–Al mixed oxide apparently results in a modification of both electronic properties of active metals and acid-base function of the catalyst surface.



## 1. Introduction

Nitrous oxide has a high global warming potential (GWP = 310) and contributes to the stratospheric ozone destruction. With increasing concerns about protecting our environment, the catalytic removal of nitrous oxide from exhausts has become very attractive. The significant anthropogenic sources of $N_2O$ are the nitric acid plants and the catalytic decomposition of nitrous oxide (Eq. (1)) belongs to the Best Available Technologies for $N_2O$ abatement from $HNO_3$ production [1].

$$N_2O \rightarrow N_2 + \tfrac{1}{2}O_2 \quad (1)$$

The high temperature catalytic decomposition (ca. 850 °C) situated immediately downstream of the ammonia burner and the "end-of-pipe" low temperature (ca. 400 °C) $N_2O$ catalytic decomposition are considered. Many different catalysts have been tested for $N_2O$ catalytic decomposition in the last four decades [2,3], especially Fe-zeolites [4–9], noble metals (Rh, Ru) on various supports [10–14], supported Cu [15–18] and mixed oxides prepared from hydrotalcite-like precursors [19–22]. Although there are first commercial catalysts available [23], there is still a space for improvement of the activity and stability of the suitable catalytic systems.

Promising results in the $N_2O$ decomposition were obtained over the mixed oxide catalysts prepared by thermal treatment of layered double hydroxides (LDHs) [24–34]. Layered double hydroxides, known also as hydrotalcite-like compounds or anionic clays, are layered materials consisting of positively charged hydroxide layers separated by interlayers composed of anions and water molecules. The chemical composition of LDHs can be represented by the general formula $[M_{1-x}^{II}M_x^{III}(OH)_2]^{x+}[A_{x/n}^{n-}\cdot yH_2O]^{x-}$ where $M^{II}$ and $M^{III}$ are divalent and trivalent metal cations, $A^{n-}$ is an $n$-valent anion, and $x$ usually has values between 0.20 and 0.33. A wide variety of LDHs can be prepared modifying both the composition of hydroxide layers and interlayer species. After heating at moderate temperatures, LDHs give finely dispersed mixed oxides of $M^{II}$ and $M^{III}$ metals with a large surface area and good thermal stability. Therefore, the LDHs are often used as precursors for the preparation of mixed oxide catalysts.

The Co–Mn–Al mixed oxide with Co:Mn:Al molar ratio of 4:1:1 has been found as the most active catalyst for $N_2O$ decomposition among all LDH-related catalysts tested by our group [35]. However, its activity was substantially decreased in the presence of water vapor [36]. For a practical use of this catalyst in low temperature $N_2O$ abatement in waste gas emitted from nitric acid production, the resistance against water inhibition, high performance in the presence of $NO_x$ ($NO + NO_2$) and long-term stability in wet acidic environment are required.

The doping of Co–Mn–Al mixed oxide by alkali metals could improve the catalytic performance as alkali metals have been

* Corresponding author. Tel.: +420 596991532; fax: +420 597323396.
*E-mail address:* lucie.obalova@vsb.cz (L. Obalová).

0926-3373/$ – see front matter © 2009 Elsevier B.V. All rights reserved.
doi:10.1016/j.apcatb.2009.03.002

found as catalyst promoters in various catalytic processes, e.g., ammonia synthesis [37], NO decomposition [38,39] and reduction [40–42], oxidative dehydrogenation of light alkanes [43,44], CO oxidation [45,46] or soot combustion [47]. In consequence of their exceptionally low ionization potentials, alkali metals can act as electronic and structural promoters, modifying the acid–base function of the surface, and due to their relatively large dimensions, possibly behave as site blocking species [48].

Alkali metals were also used to promote catalysts for $N_2O$ decomposition, e.g., $Rh/Al_2O_3$ [49,50], $Co_3O_4$ [51–54] and $Co_3O_4$–$CeO_2$ [55]. A small amount of alkali metals was also found out to promote the decomposition of $N_2O$ over catalysts prepared by calcination of hydrotalcite-like compounds [24,56].

Since the hydrotalcite structure allows a controlled insertion of different elements during the catalyst preparation, the possible development of synergic interactions between catalytically active metals and different promoters can be investigated. In this work, the Co–Mn–Al mixed oxide doped with various amount of K was studied as catalyst of $N_2O$ decomposition with the aim to discuss the relationship between catalytic performance and K content. Although some works regarding the influence of alkali promoters on the activity of $N_2O$ decomposition catalysts have been published, the experiments were performed only in the inert gas [46,48,51] or in the presence of oxygen and/or water vapor [49,50]. However, $NO_x$ are always present simultaneously with $N_2O$ in off-gases. Therefore, this work is focused on the determination of $H_2O$, $O_2$, NO and $NO_2$ influence to test the suitability of K-doped Co–Mn–Al mixed oxide catalyst for $N_2O$ decomposition in a real off-gas from nitric acid plant.

## 2. Experimental

### 2.1. Catalysts preparation

The Co–Mn–Al layered double hydroxide with Co:Mn:Al molar ratio of 4:1:1 was prepared by coprecipitation of corresponding nitrates in an alkaline $Na_2CO_3$/NaOH solution at 25 °C and pH 10. The resulting suspension was stirred at 25 °C for 1 h; the product was then filtered off and thoroughly washed with distilled water. The washed filtration cake was re-suspended in a solution of $KNO_3$, which concentration was adjusted to obtain a desired concentration of potassium in mixed oxide. The product was again filtered off, dried at 105 °C and calcined for 4 h at 500 °C in air. Finally, the sample was crushed and sieved to obtain a fraction with particle size of 0.160–0.315 mm. The catalyst samples, i.e., K-modified Co–Mn–Al mixed oxides were denoted according to their promoter content determined by chemical analysis (e.g., 0.9% K means Co–Mn–Al mixed oxide catalyst modified by ca. 0.9 wt% of potassium).

### 2.2. Catalysts characterization

Powder X-ray diffraction patterns were recorded using a Seifert XRD 3000P instrument with Co Kα radiation ($\lambda$ = 0.179 nm, graphite monochromator, goniometer with Bragg-Brentano geometry) in $2\theta$ range 10–120°, step size 0.02°. For refinement of lattice parameters and estimation of the mean coherence length (approximately equal to crystallite size), DiffracPlus Topas, release 2000 (Bruker AXS, Germany) was used. The structural models were taken from the Inorganic Crystal Structure Database ICSD, Retrieve 2.01 (FIZ Karlsruhe, Germany).

The X-ray photoelectron spectra were measured using ESCA 310 (Gammadata Scienta, Sweden) photoelectron spectrometer. The measurements were performed using Al Kα radiation for electron excitation. The FWHM of Au $4f_{7/2}$ photoemission line of bulk Au standard was 0.65 eV. The samples were spread on a gold support and spectra were recorded at room temperature and pressure of $6 \times 10^{-8}$ Pa. The surface static charging of the samples was suppressed by using a Scienta flood gun. The following photoelectrons were recorded: Co 2p, Co 3p, Mn 2p, K 2p, Al 2p, Al 2s, C 1s and O 1s. Quantification of the elements concentrations was accomplished by correcting photoelectron peak intensities for their cross-sections [57].

The surface area and porous structure of the prepared catalysts were determined by adsorption/desorption of nitrogen at −196 °C using ASAP 2010 instrument (Micromeritics, USA) and evaluated by BET method and BJH methods, respectively. Prior to the measurement, the samples were dried in a drying box at 120 °C for at least 12 h, then evacuated in the ASAP instrument.

Temperature-programmed reduction (TPR) measurements were carried out to find out reducibility of the catalysts. Experiments were performed with a sample amount of 0.025 g, a $H_2/N_2$ mixture (10 mol% $H_2$), flow rate 50 ml $min^{-1}$ and linear temperature increase 20 °C $min^{-1}$ up to 1000 °C. A change in $H_2$ concentration was detected with a mass spectrometer Omnistar 300 (Pfeiffer Vacuum). Reduction of the grained CuO (0.16–0.315 mm) was repeatedly performed to calculate absolute values of the hydrogen consumed during reduction.

Temperature-programmed desorption (TPD) of $NH_3$ and $CO_2$ was carried out with a sample amount of 0.050 g, to examine acid and basic properties of the catalysts, respectively. The measurements were accomplished in the temperature range 20–1000 °C, with helium as a carrier gas and $CO_2$ or $NH_3$ as adsorbing gases. The heating rate 20 °C $min^{-1}$ was applied. During the experiments the following mass contributions *m/z* were collected: 2-$H_2$, 18-$H_2O$, 16-$NH_3$, and 44-$CO_2$. The spectrometer was calibrated by dosing an amount (840 μl) of $CO_2$ or $NH_3$ into the carrier gas (He) in every experiment. The TPR and TPD experiments were evaluated using OriginPro software with an accuracy of ±5%.

### 2.3. Catalytic measurements

Catalytic measurements of $N_2O$ decomposition were performed in an integral fixed bed stainless steel reactor of 5 mm internal diameter in the 300–450 °C temperature range and atmospheric pressure. Feed to the reactor contained 0.1 mol% $N_2O$, oxygen (0–5 mol%), NO (0–0.17 mol%), $NO_2$ (0–0.17 mol%) and water vapor (0–4 mol%) balanced by helium. The amount of catalyst used in the catalytic measurements was 0.1–0.3 g. Average bulk density of the catalyst grains was 0.673 g $cm^{-3}$. The space velocity (GHSV) varied between 40 380–13 460 $h^{-1}$. The reactor was heated by a temperature-controlled furnace. An absorption tower at ambient temperature was used for humidification of the helium flow and the experimental apparatus was equipped by a heated line to avoid water condensation. Before each run, the catalyst was pre-treated by heating in a He flow (100 ml $min^{-1}$) at 10 °C $min^{-1}$ up to 450 °C and maintained at this temperature for 1 h. Then the catalyst was cooled to the reaction temperature and the steady state of the $N_2O$ concentration level was measured. A GC/TCD was used to analyze $N_2O$ concentration and $O_2/N_2$ molar ratio at the reactor outlet and inlet. The chromatographic column PoraPlot Q (30 m × 0.53 mm × 40 μm) and Molsieve 5A (30 m × 0.53 mm × 25 μm) were used. Data were acquired with HP Chemstation. IR analyzer (Ultramat 6, Siemens) equipped with $NO_2$/NO converter was used for NO and $NO_2$ analysis. The content of the water vapor was determined from the measurements of temperature and relative humidity.

## 3. Results and discussion

### 3.1. Characterization of catalysts

The Co:Mn:Al molar ratio in the catalysts determined by chemical analysis (AAS) corresponded approximately to the ratio

**Table 1**
Bulk and surface analysis of the Co–Mn–Al mixed oxide catalysts modified by different amount of K.

| Sample | K (wt%) | | Co (wt%) | | Mn (wt%) | | Al (wt%) | | Na (wt%) | Molar ratio Co:Mn:Al | |
|---|---|---|---|---|---|---|---|---|---|---|---|
| | AES | XPS | AAS | XPS | AAS | XPS | AAS | XPS | AAS | AAS | XPS |
| 0% K | 0 | 0 | 52.0 | 48.0 | 10.7 | 9.6 | 5.70 | 8.2 | 0.110 | 4:0.88:0.96 | 4:0.86:1.50 |
| 0.2% K | 0.16 | 0.719 | 52.0 | 48.0 | 10.5 | 9.3 | 5.51 | 8.8 | 0.058 | 4:0.87:0.93 | 4:0.83:1.60 |
| 0.4% K | 0.40 | 1.348 | n.d. | 49.3 | n.d. | 8.9 | n.d. | 7.9 | 0.071 | n.d. | 4:0.77:1.40 |
| 0.9% K | 0.92 | 3.200 | n.d. | 45.6 | n.d. | 10.8 | n.d. | 8.9 | 0.066 | n.d. | 4:1.03:1.60 |
| 1.6% K | 1.60 | 4.366 | 51.1 | 44.2 | 10.5 | 10.6 | 5.66 | 8.1 | 0.063 | 4:0.88:0.97 | 4:1.02:1.71 |
| 2.7% K | 2.72 | n.d. | n.d. | n.d. | n.d. | n.d. | n.d. | n.d. | 0.052 | n.d. | n.d. |
| 3.0% K | 2.99 | 7.778 | 48.0 | 40.7 | 9.94 | 10.5 | 5.26 | 7.9 | 0.056 | 4:0.89:0.96 | 4:1.11:1.69 |

of 4:1:1, i.e., to the value adjusted in nitrate solution used for coprecipitation; the content of potassium varied from 0 to 3 wt% (Table 1). Moreover, a slight amount of residual Na cations was also present in all samples. Sodium can also act as a promoter for $N_2O$ decomposition but its effect is supposed to be negligible in this particular case with low Na contents, only sample 0% K is the exception due to the sodium content of 0.11 wt%.

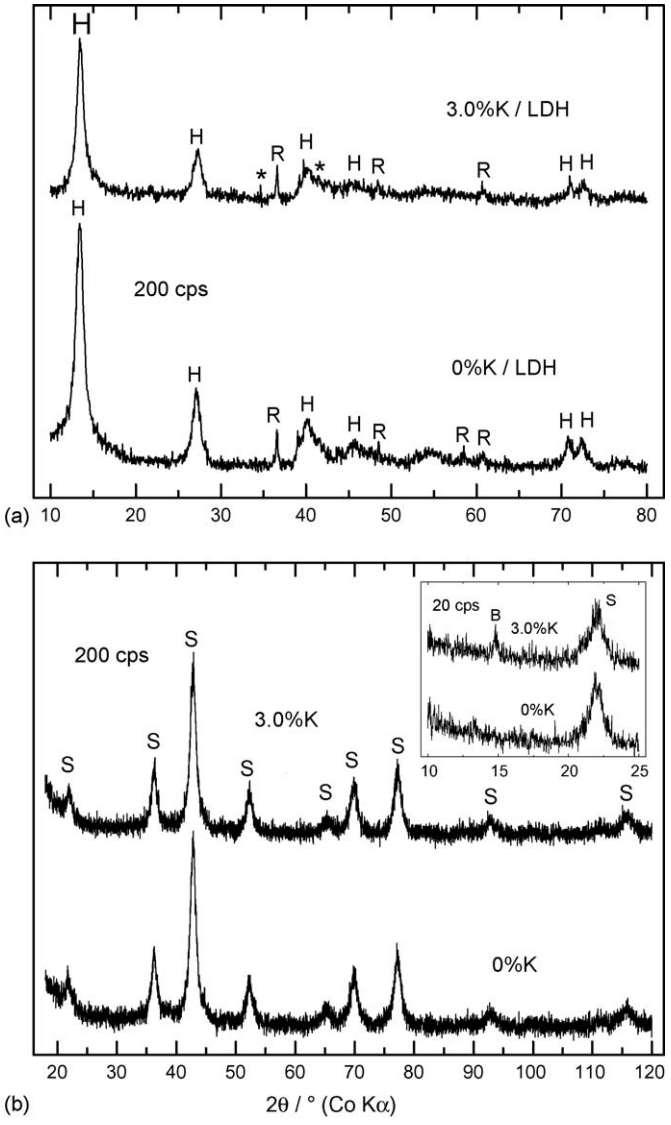


**Fig. 1.** Powder XRD patterns of the dried Co–Mn–Al LDH precursors (a) and related mixed oxides (b) prepared by calcination at 500 °C. H, hydrotalcite-like phase; R, $MnCO_3$ (rhodochrosite); *, $KNO_3$; S, Co–Mn–Al spinel; B, birnessite-like phase.

In the powder XRD patterns of the prepared precursors, a well-crystallized hydrotalcite-like phase was found (Fig. 1a). A slight amount of $MnCO_3$ (rhodochrosite) admixture was also detected in all precursors. The modification of LDH precursors with potassium did not change their phase composition; only traces of $KNO_3$ were detected in the sample with the highest concentration of potassium. After calcination of the precursors at 500 °C, the Co–Mn–Al mixed oxide with spinel structure was obtained (Fig. 1b). Spinel-type oxides are the primary crystallization products during thermal treatment of the cobalt-containing LDHs; a segregation of Co-enriched spinels of $Co_3O_4$ type with a gradual incorporation of Mn and Al into the spinel lattice at moderate calcination temperatures can be expected in the Co–Mn–Al systems [58]. An incorporation of potassium into the solid led to some changes in the XRD patterns: The spinel lattice parameter $a$ and the mean coherence length (approximately equal to the crystallite size) varied in the range 0.808–0.811 nm and 7.3–10.2 nm, respectively. The error of the Rietveld refinement was larger than a possible variation of these parameters on the changing K content, i.e., no statistically significant dependence of the lattice parameter and crystallite size on the catalysts composition was found. In the samples with high content of potassium (2.7 and 3.0% K), a trace amount of birnessite-type oxide, $K_xMnO_2$, was detected. The characteristic birnessite diffraction peak at $d \sim 0.7$ nm in the 3.0% K sample is demostrated in Fig. 1b.

The BET surface area of Co–Mn–Al mixed oxide catalysts with various K contents changed only slightly, while some changes of average pore diameter ($4V/S_{BET}$) were observed (Table 2). No direct dependency of the catalytic activity on the surface area was found. Also Asano et al. [52] concluded that the activity of K-doped $Co_3O_4$ catalysts for $N_2O$ decomposition did not depend on the catalyst surface area although an increase in BET surface was observed after modification of $Co_3O_4$ catalyst with potassium.

The XPS data provide information about samples composition, obtained from core photoemission intensity data, and information about the chemical state of the elements in the near-surface region. The detailed XPS analysis of Co–Mn–Al mixed oxide without K modifications based on the comparison of catalyst and oxide standards was published in our previous work [35]. An analysis of the Mn 2p photoelectron spectra showed that manganese occurs as $Mn^{3+}$ and $Mn^{4+}$ with $Mn^{3+}/Mn^{4+}$ ratio of 2.27. A presence of several

**Table 2**
Analysis of porous structure of the Co–Mn–Al mixed oxide catalysts modified by different amount of K.

| Sample | $S_{BET}$ ($m^2$/g) | $V_{meso}$ ($cm^3$/g) | $4V/S_{BET}$ (nm) |
|---|---|---|---|
| 0% K | 89 | 0.48 | 18.8 |
| 0.2% K | 108 | 0.43 | 15.0 |
| 0.4% K | 101 | 0.38 | 14.0 |
| 0.9% K | 96 | 0.44 | 12.3 |
| 1.6% K | 103 | 0.43 | 15.5 |
| 2.7% K | 99 | 0.41 | 15.7 |
| 3.0% K | 93 | 0.39 | 15.5 |

components was also recognized from Co 2p photoelectron spectra. They reveal the presence of both, $Co^{2+}$ and $Co^{3+}$ oxidation states in the ratio $Co^{2+}/Co^{3+}$ of 1.13.

The modification of Co–Mn–Al mixed oxide catalyst by different contents of potassium caused no significant changes in the values of binding energies (BE), shape and width of the Mn 2p and Co 2p photoelectron spectra. The binding energies for Mn $2p_{3/2}$ and Co $2p_{3/2}$ were $642.1 \pm 0.05$ and $780.2 \pm 0.05$ eV, respectively. The binding energy for the K $2p_{3/2}$ line was determined as $292.9 \pm 0.1$ eV with the exception of the 3.0% K sample. The binding energy of potassium in the 3.0% K sample was lower, 292.7 eV; this is probably related to the formation of a birnessite-type phase detected by the XRD in samples with a high K content. According to the literature [38,50,52,55], the negative BE shift indicates an increase in electron density of potassium and its stronger interaction with lattice oxygen, which may be related to the formation of the new phase. Only weakly bonded species K–O–Co(Mn) are proposed in the sample with lower K content [59]. Also Asano [52] observed the BE shift of the K 2 $p_{3/2}$ peak with an increasing K loading in the $Co_3O_4$ catalyst; however, the K $2p_{3/2}$ shifted to the higher binding energy with an increasing K loading and it was attributed to the interaction of potassium ions with the surface hydroxide ions. Although we also expected shifts of the Co $2p_{3/2}$, Mn $2p_{3/2}$ and O 1s BE as the counter of the K $2p_{3/2}$ BE shift and in accordance of literature results [38,48,50,51], these subtle changes were probably covered by XPS experimental error. For instance Asano et al. [52] reported that the Co $2p_{3/2}$ peak slightly shifted toward the lower BE side by the addition of a small amount of K to the $Co_3O_4$ catalyst, indicating a change in the electronic state of Co to the lower valence state and weakening of the Co–O bond strength [38].

The relation between bulk and surface concentration of potassium shows nearly linear dependence (Fig. 2) indicating that surface concentration is almost three times higher in comparison with bulk one. Similar results were also observed by other authors [38,50]. We suppose that almost all potassium is present on the catalyst surface because during the preparation of the catalysts, potassium was added to the coprecipitated Co–Mn–Al hydrotalcite and no significant migration to the bulk is expected due to the big cationic radius of $K^+$. From data in Table 1 implies that surface concentrations of cobalt is lower than bulk; Mn concentration on the surface slightly increases with increasing bulk concentration of potassium, and surface concentration of Al is 1.5× higher than that in the bulk as has been already published [35].

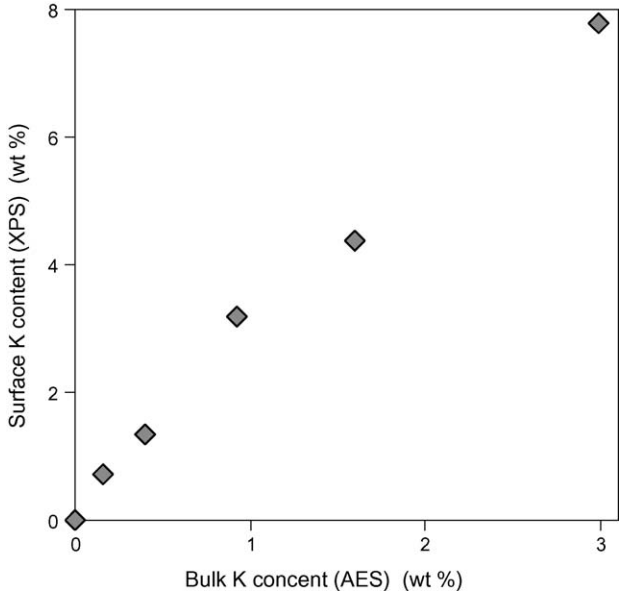


**Fig. 2.** Dependence of surface K concentration on the bulk K concentration in Co–Mn–Al mixed oxide doped with K.

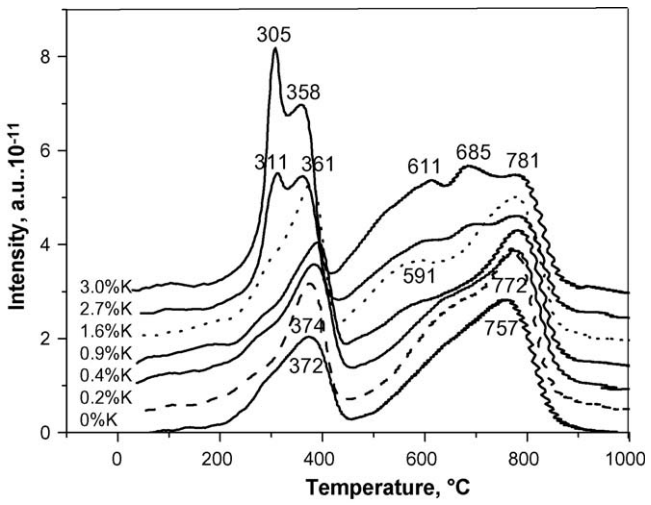


**Fig. 3.** Temperature-programmed reduction results of the Co–Mn–Al mixed oxide catalyst modified by various amount of potassium.

The TPR patterns showed differences in reducibility of the prepared catalysts caused by the modification with K (Fig. 3). The non-modified Co–Mn–Al catalyst was reduced in two main temperature regions, 200–400 °C and 400–900 °C. Both reduction peaks consist of overlapping peaks corresponding to the co-effect of more species. According to the results of Ribet et al. [60], Arnoldy et al. [61] and our previously published results [35], the low-temperature reduction peak represents the reduction of $Co^{III} \rightarrow Co^{II} \rightarrow Co^0$ in $Co_3O_4$ like phase. The reduction of $Mn^{IV}$ species cannot be excluded in this temperature region. Generally, reduction of manganese species proceeds in steps $Mn^{IV} \rightarrow Mn^{II,III} \rightarrow Mn^{II}$ at temperatures lower than 1200 °C [62] and corresponding temperature regions are strongly dependent on the sample crystallinity. Our unpublished results showed that electrochemical $MnO_2$ (TOSOH, Greece) was reduced in the temperature range 200–600 °C and $MnO_2$ from Aldrich (a crystalline form of pyrolusite was confirmed by XRD) was reduced in the temperature range 400–800 °C. This makes the identification of Mn species based on the TPR of Mn oxide standards very difficult.

The high temperature peak was attributed to the reduction of Co and Mn ions surrounded by Al ions in a spinel-like phase. It is well known that the number of Al cations in the surrounding of the Co ones mainly determines the TPR reduction temperature, while the Co valency and coordination are less important; this phenomenon can be explained by polarization of the more or less covalent Co–O bonds by Al cations. This will increase the effective charge of the Co cations and, as a consequence, the lattice energy, resulting in an increase of reduction temperature [61].

The modification of the Co–Mn–Al mixed oxide by K caused only a slight shift of both reduction peaks. With increasing K content a shift of the low-temperature reduction peaks to lower temperatures was observed. The high temperature peak became broader with increasing K content and a new maximum appeared at around 580–620 °C.

For the 2.7% K and 3.0% K samples a new reduction peak was clearly visible in the low temperature region, though some indication of its presence can be found in the samples with lower K concentration. The same new reduction peak in TPR patterns of calcined Co–Al LDH modified by K was observed by Cheng et al. [56]. They assigned it to the reduction of $KNO_3$ or $KNO_2$. Regarding

**Table 3**
Results of TPD and TPR analysis of the Co–Mn–Al mixed oxide catalysts modified by different amount of K.

| Sample | TPD $CO_2$ (mmol/g), 25–500 °C | TPD $NH_3$ (mmol/g), 25–500 °C | TPR $H_2$ (mmol/g), 25–1000 °C | TPR $H_2$ (mmol/g), 1st peak | TPR $H_2$ (mmol/g), 2nd peak |
|---|---|---|---|---|---|
| 0% K | 0.053 | 0.313 | 16.29 | 4.88 | 11.42 |
| 0.2% K | 0.160 | 0.489 | 14.10 | 4.17 | 9.93 |
| 0.4% K | 0.139 | 0.458 | 13.79 | 4.40 | 9.40 |
| 0.9% K | 0.462 | 0.238 | 13.32 | 4.18 | 9.14 |
| 1.6% K | 0.349 | 0.157 | 14.93 | 4.74 | 10.19 |
| 2.7% K | 0.901 | 0.180 | 12.92 | 4.22 | 8.69 |
| 3.0% K | 0.775 | 0.068 | 16.93 | 5.73 | 11.20 |

the fact that we have already observed this peak also at TPR patterns of some other Co–Mn–Al mixed oxides (without potassium) and that $KNO_3$ reduction started at 740 °C under our TPR conditions, we tried to find another explanation for the findings. We excluded birnessite (determined by XRD in the samples); the reference birnessite sample started to reduce at about 300 °C with maximum at 470 °C. According to Arnoldy [61], peak at 300 °C can be attributed to $H_2$-assisted decomposition of Co nitrate species. This hypothesis is in accord with our results: NO evolution was observed at 300 °C, TPR maxima of reference $Co(NO_3)_2$ were detected at 268 and 321 °C (not shown here). However, in the same temperature region we observed also reduction of reference $Na_2O_2$ (TPR maxima at 200 and 360 °C). According to Fierro et al. [63] the new low-temperature peak may be also related to a different kinetics of the reduction process, i.e., surface oxygen involving reduction. The amounts of hydrogen consumed at the reduction of the catalyst samples are given in Table 3. The hydrogen consumption does not substantially change, within the experimental error, with increasing the amount of potassium, as well as its distribution between low- and high-temperature peaks.

Alkali cations are Lewis acids and have no electron donation effects. However, they increased the basicity of oxygen anions in their coordination sphere [48] under formation of anionradical $O_2^-$ [64], which is in turn reflected in the increase of basicity of the Co–Mn–Al mixed oxide catalyst with increasing potassium content (Fig. 4). Increasing basicity (amount of desorbed $CO_2$ determined by TPD) is connected with decreasing acidity (amount of desorbed $NH_3$ determined by TPD).

### 3.2. $N_2O$ decomposition in inert gas

The temperature dependences of $N_2O$ conversion are shown in Fig. 5. Modification of the Co–Mn–Al mixed oxide catalyst by different amount of potassium significantly changed its catalytic activity. The temperature dependency of $N_2O$ conversion showed that the most active samples are 1.6% K and 0.9% K. Their activity is nearly the same taking the experimental error into account. The dependence of $N_2O$ conversion (390 and 450 °C) on the surface K content is showed in Fig. 6. An increasing activity with a rising content of potassium up to 0.9–1.6 wt% K, after that a gradual decrease of $N_2O$ conversion was observed.

Based on information published in literature [2,65] and our recent results [66], a redox mechanism of $N_2O$ decomposition can be considered. The oxidation of the catalyst surface by $N_2O$ molecule is the first step of the reaction; the second step is oxygen desorption according to the Langmüller or Eley-Rideal mechanisms; the latter is proposed to prevail over calcined hydrotalcites [66,67]. Active catalysts have to allow both a fast $N_2O$ chemisorption and a fast desorption of oxygen. Therefore, the ability of an active site to offer charge into the $N_2O$ antibonding orbital and the ability of the catalyst surface to be reduced easily are two predominant assumptions: An optimum strength of the oxygen–metal bond is required for a very active $N_2O$ decomposition catalyst. The strength of the oxygen–metal bond can be determined from the TPR experiment as a shift of the reduction peak maximum to lower temperatures.

Previous publications imply that potassium acts as an electron promoter and a modification by potassium causes an increase in

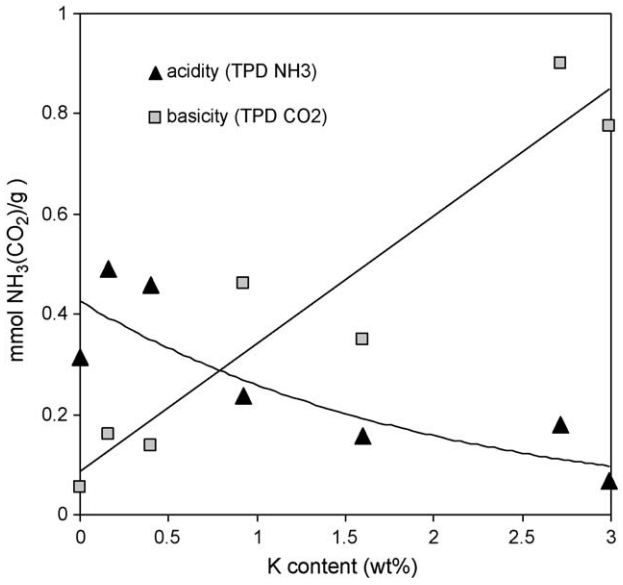


**Fig. 4.** Dependence of basicity (expressed as a desorbed amount of $CO_2$ at 25–500 °C) and acidity (expressed as a desorbed amount of $NH_3$ at 25–500 °C) on the potassium content in the Co–Mn–Al mixed oxide.

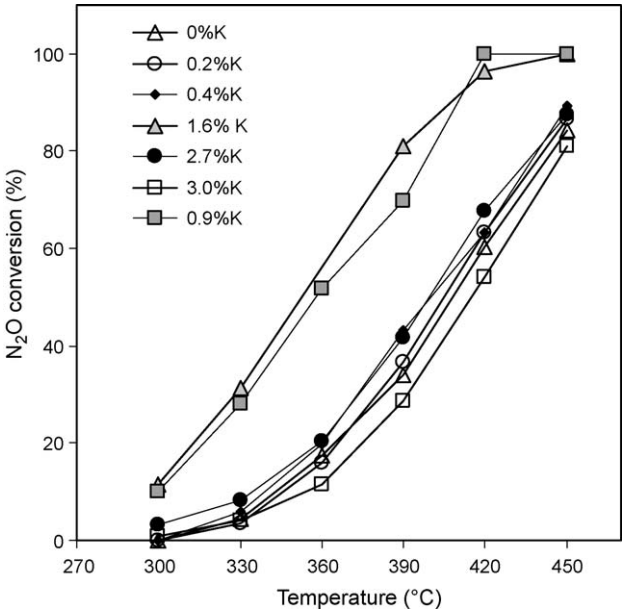


**Fig. 5.** Temperature dependence of $N_2O$ conversion over Co–Mn–Al mixed oxide catalysts modified by K. Conditions: 0.1 mol% $N_2O$ in He, GHSV = 40 380 $h^{-1}$.

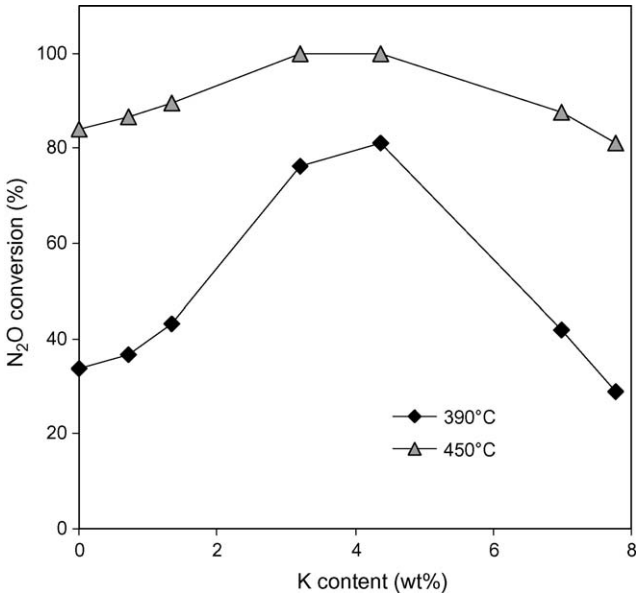


**Fig. 6.** Dependence of $N_2O$ conversion on the surface potassium concentration in Co–Mn–Al mixed oxide. Conditions: 0.1 mol% $N_2O$ in He, GHSV = 40 380 $h^{-1}$.

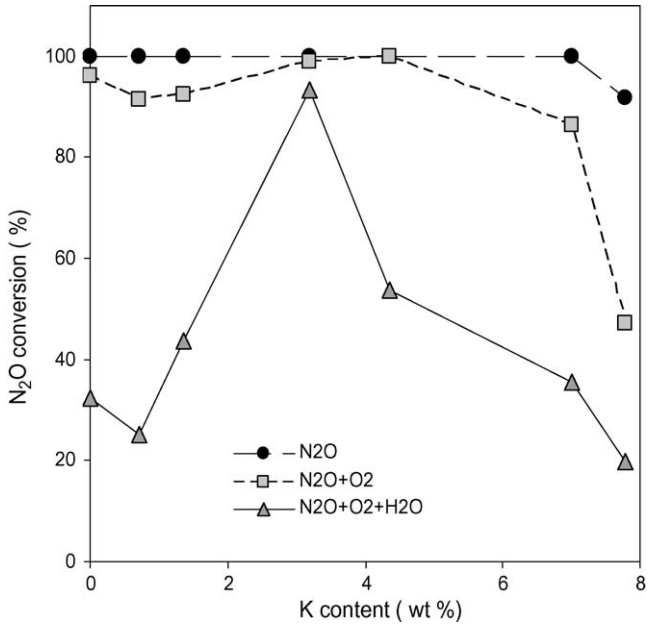


**Fig. 7.** The dependence of $N_2O$ conversion on the surface potassium concentration in the dry and the wet stream. Conditions: 450 °C, GHSV = 13 460 $h^{-1}$; $N_2O$: 0.1 mol% $N_2O$, rest He; $N_2O + O_2$: 0.1 mol% $N_2O$, 5 mol% $O_2$, rest He; $N_2O + O_2 + H_2O$: 0.1 mol% $N_2O$, 5 mol% $O_2$, 4 mol% $H_2O$, rest He.

the electron density of the transition metal [38,45,52,53]. Differences of catalytic activity in inert gas may be related to the changes of oxygen–transition metal bond strength observed from the shift of TPR maxima and more general to the changes of electron work function related to the formation of surface dipoles [53,68]. Optimal potassium content facilitates the redox processes occurring between catalyst surface and the reaction intermediates produced during the $N_2O$ decomposition. When potassium ions come closer due to gradual increase in their concentration, mutual depolarization takes place, and after passing the minimum, the work function starts to increase with the amount of potassium added [53].

### 3.3. Effect of oxygen and water vapor on $N_2O$ decomposition

The effect of oxygen and water vapor on $N_2O$ decomposition at 450 °C is demonstrated in Fig. 7. Presence of oxygen in $N_2O$ caused maximum 10 rel.% decrease in $N_2O$ conversion when the catalysts contained less than 1.6 wt% K, whereas high concentration of K (3 wt%) in the catalyst caused substantial decrease in catalytic activity. The presence of water and oxygen in the feed decreased the catalyst activity substantially compared to the presence of oxygen only.

It is seen that the dependence of $N_2O$ conversion in the presence of $O_2$ and $H_2O + O_2$ on the K content showed a similar volcano-type curve as the dependence of $N_2O$ conversion in the water- and oxygen-free feed gas (Fig. 6). It means, the more the catalyst is active in helium, the more active it is in the presence of water vapor and oxygen. The negative effects of $O_2$ and $H_2O$ are accumulative. This has been already observed in our earlier work dealing with the effect of water vapor and oxygen on the catalytic activity of Co–Mg–Mn–Al mixed oxide catalyst for $N_2O$ decomposition [36] and in other works dealing with $N_2O$ decomposition over calcined hydrotalcites [19,69]. The exception in volcano-type curve was a slightly higher activity of 0% K sample in the presence of $O_2$ and $O_2 + H_2O$ than 0.2% K one, probably due to the content of residual sodium in 0% K catalyst.

In both cases, $O_2$ and $H_2O$ inhibition, the lowering of the activity is fully reversible and the activity can be completely recovered when water and oxygen are eliminated from the feed. This implies that oxygen and especially water does not induce drastic structural changes as e.g. in the case of some zeolites [70–72].

The competitive adsorption of the $H_2O$ and $N_2O$ at the same active sites is the proposed mechanism of water vapor inhibition, since $H_2O$ and $N_2O$ are both polar molecules and use the oxygen end of molecules to strike transition metal cations [2,52,67,73]. Generally, the presence of water in the feed does not always affect the extent of the reaction [2,74]. Given that the adsorption of water is exothermal, inhibition caused by water is observed at low temperatures, whereas the activity at high temperatures is not affected. Surprisingly, positive effect of water vapor presence was also found [73,75].

It can be concluded that the extent of oxygen and water vapor inhibition depends on the actual O and OH surface active site coverage. It was, in the case of K-promoted Co–Mn–Al mixed oxide, influenced by potassium content. No direct dependency of water and oxygen inhibition on the acido-basic properties was found.

### 3.4. Effect of oxygen and $NO_x$ on $N_2O$ decomposition

The dependence of $N_2O$ conversion in the feed containing $NO_x$ and $O_2$ on the potassium content in the Co–Mn–Al mixed oxide is shown in Fig. 8. The influence of NO and $NO_2$ gases on the $N_2O$ decomposition rate was examined because the waste gases from nitric acid production contained NO and $NO_2$ in 1:1 ratio. High concentrations of NO and $NO_2$ were chosen to test the stability of catalysts in aggressive conditions. These conditions corresponded approximately to the gas composition entering the selective catalytic reduction of $NO_x$ in a nitric acid plant. All tested catalysts showed no deactivation during catalytic measurements.

It was found that $N_2O$ conversion over the non-modified Co–Mn–Al mixed oxide (0% K sample) is only very slightly influenced by NO, $NO_2$ and their mixture with $O_2$. Completely different results were obtained over the Co–Mn–Al catalysts modified by potassium. The NO presence caused a decrease of $N_2O$ conversion; this decrease was becoming higher with the increasing amount of potassium. Similarly, the presence of $NO_2$ also caused a decrease of the $N_2O$ conversion; however this decrease was greater than in the

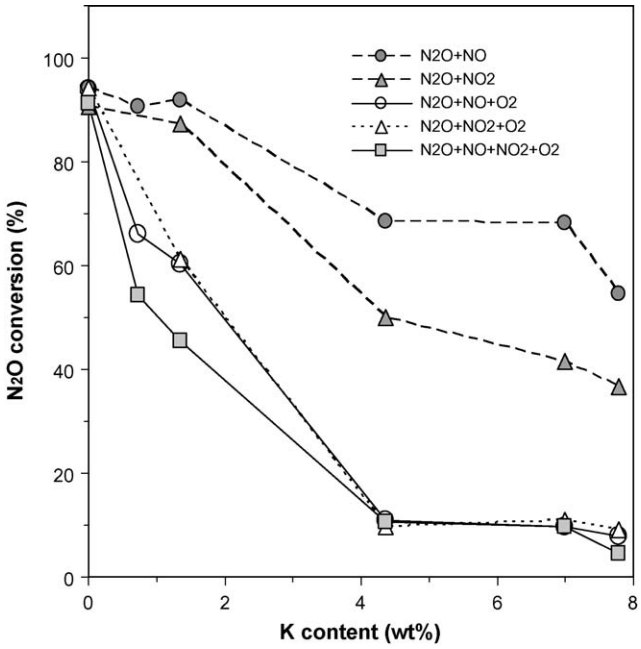


**Fig. 8.** The dependence of $N_2O$ conversion on the surface potassium concentration in the presence of $NO_x$ and oxygen. Conditions: 450 °C, GHSV = 13 460 $h^{-1}$, $N_2O$ + NO: 0.1 mol% $N_2O$, 0.17 mol% NO, rest He; $N_2O$ + $NO_2$: 0.1 mol% $N_2O$, 0.17 mol% $NO_2$, rest He; $N_2O$ + $NO_2$ + $O_2$: 0.1 mol% $N_2O$, 0.17 mol% $NO_2$, 5 mol% $O_2$, rest He; $N_2O$ + NO + $O_2$: 0.1 mol% $N_2O$, 0.17 mol% NO, 5 mol% $O_2$, rest He; $N_2O$ + NO + $O_2$: 0.1 mol% $N_2O$, 0.17 mol% NO, 5 mol% $O_2$, rest He.

case of NO. A significant decrease of the $N_2O$ conversion was found when oxygen was also present. It is interesting that in all three cases ($N_2O$ + NO + $O_2$, $N_2O$ + $NO_2$ + $O_2$ and $N_2O$ + NO + $NO_2$ + $O_2$) the $N_2O$ conversions are the same when experimental error is considered. The competitive adsorption of NO on the same active site as $N_2O$ can be assumed [2]. Moreover, our experiments showed that the NO catalytic oxidation (Eq. (2))

$$NO + \tfrac{1}{2}O_2 \rightarrow NO_2 \quad (2)$$

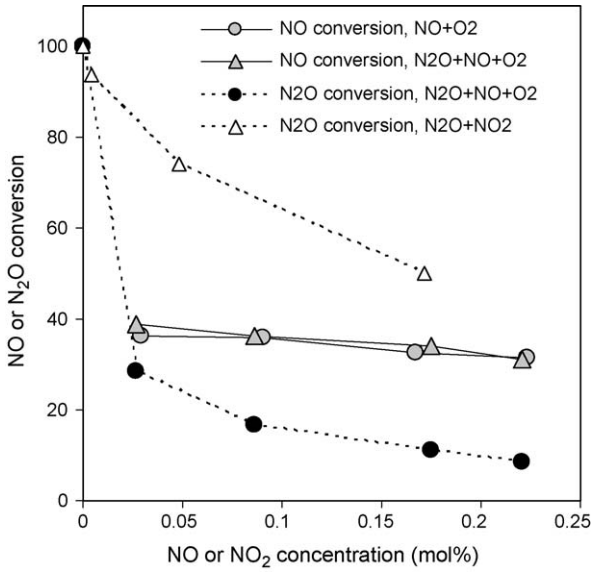


**Fig. 9.** The dependence of $N_2O$ and/or NO conversion on the NO or $NO_2$ concentration in the feed over 1.6% K catalyst.
Conditions: 450 °C, GHSV = 13 460 $h^{-1}$; NO + $O_2$: 0.03–0.22 mol% NO, 5 mol% $O_2$, rest He; $N_2O$ + NO + $O_2$: 0.1 mol% $N_2O$, 0–0.22 mol% $NO_2$, 5 mol% $O_2$, rest He; $N_2O$ + $NO_2$: 0.1 mol% $N_2O$, 0–0.17 mol% $NO_2$, rest He.

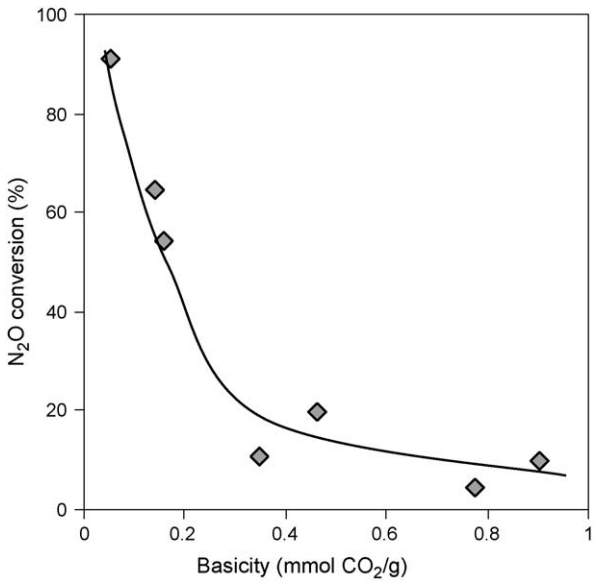


**Fig. 10.** The dependence of $N_2O$ conversion in the presence of NO, $NO_2$ and $O_2$ on the basicity of K-modified Co–Mn–Al mixed oxide catalysts.
Conditions: 450 °C, GHSV = 13 460 $h^{-1}$, 0.1 mol% $N_2O$, 0.17 mol% $NO_2$, 0.17 mol% NO, 5 mol% $O_2$, rest He.

occurs both in the presence of $N_2O$ and in the inert only, while the attained NO conversions are equal in both cases (Fig. 9). This implies that the presence of $N_2O$ has no effect on the NO oxidation process. On the contrary, the decomposition of $N_2O$ is influenced by the presence of NO and $NO_2$: an increasing amount of both NO and $NO_2$ caused a decrease in $N_2O$ conversion (Fig. 9).

Further work is in progress to elucidate the $N_2O$ inhibition mechanism by $NO_x$ in the excess of oxygen and the extent of NO and $NO_2$ adsorption related to the K content in the Co–Mn–Al mixed oxide. However, based on the results obtained up to now, it can be concluded that catalysts with low potassium content, which exhibited low basicity of the surface (determined as the desorbed

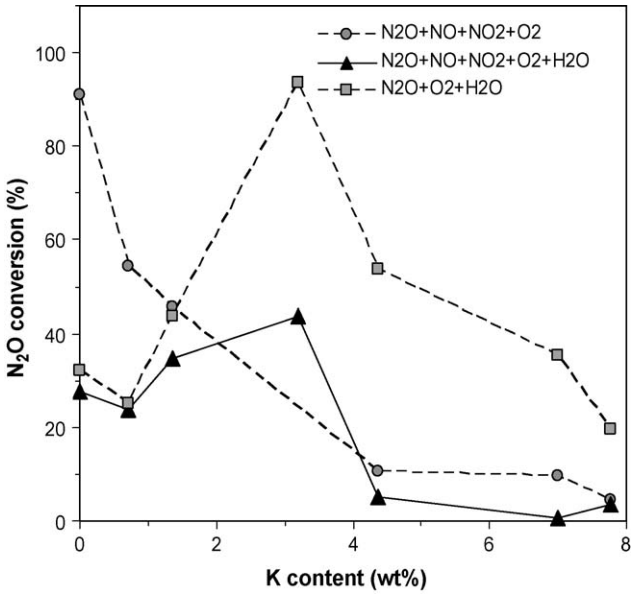


**Fig. 11.** The dependence of $N_2O$ conversion on the surface potassium concentration in the presence of oxygen, water vapor and $NO_x$.
Conditions: 450 °C, GHSV = 13 460 $h^{-1}$, $N_2O$ + NO + $NO_2$ + $O_2$: 0.1 mol% $N_2O$, 0.17 mol% NO, 0.17 mol% $NO_2$, 5 mol% $O_2$, rest He; $N_2O$ + NO + $NO_2$ + $O_2$ + $H_2O$: 0.1 mol% $N_2O$, 0.17 mol% NO, 0.17 mol% $NO_2$, 5 mol% $O_2$, 4 mol% $H_2O$, rest He; $N_2O$ + $O_2$ + $H_2O$: 0.1 mol% $N_2O$, 5 mol% $O_2$, 4 mol% $H_2O$, rest He.

amount of $CO_2$ from the TPD experiments) adsorbed possibly less acidic $NO_x$ gases and consequently had a higher catalytic activity in the presence of $NO_x$. The dependence of $N_2O$ conversion in the presence of NO, $NO_2$ and $O_2$ on the basicity of the K-modified Co–Mn–Al mixed oxide is shown in Fig. 10.

### 3.5. Effect of oxygen, water vapor and $NO_x$ on $N_2O$ decomposition

The results above imply that an optimum content of potassium is necessary for the high $N_2O$ decomposition activity in the presence of water vapor and oxygen (Fig. 7). Appropriate redox properties of the catalyst required for a high reaction rate of $N_2O$ decomposition can be achieved by the use of an optimal promoter amount. On the other hand, the high catalytic efficiency in the presence of $NO_x$ and $O_2$ can be achieved by setting suitable acidic-basic properties of the catalyst surface. In order to achieve the high activity in the presence of $NO_x$ and $O_2$, it is necessary for the basic properties to be as low as possible. In this case the Co–Mn–Al mixed oxide without any potassium modifications meets the criterion of the lowest basicity (Fig. 10). For a good catalytic performance under both conditions ($N_2O + O_2 + H_2O + NO + NO_2$), the optimal K content ca. 0.9 wt% was determined (Fig. 11).

## 4. Conclusions

The Co–Mn–Al mixed oxide modified by different amount of potassium was tested for $N_2O$ decomposition under various feed compositions. The catalyst without K modification was the most active in the presence of $O_2$ and $NO_x$, and contained the smallest amount of basic components. The $N_2O$ conversion decreased gradually with increasing potassium content and the increase of surface basicity was observed at the same time. For the high catalytic activity in the presence of $H_2O$, the optimum amount of potassium promoter is required. This is connected with optimum redox properties of the catalyst. The observed dependencies are in relation to the hypothetical mechanism of $N_2O$ decomposition.

The potassium modification can serve as a chemical tool for adjusting the bifunctional properties of the Co–Mn–Al mixed oxide catalyst because K can acts as an electronic promoter, simultaneously modifying the acid–base function of the surface. The abatement of $N_2O$ emission from nitric acid plants is the main practical application of low temperature $N_2O$ catalytic decomposition presented in this paper. The catalytic reactor for $N_2O$ decomposition can be situated upstream of the selective catalytic reduction of $NO_x$ where relative high temperature but also high $NO_x$ concentration is. Other possibility is to place the SCR $NO_x$ downstream where lower $NO_x$ concentration but also lower temperature occurs (end-of-pipe solution) [23]. The catalyst containing ca. 0.9 wt% K was the most active one under the conditions simulating the composition of the waste gas upstream of the SCR $NO_x$ unit in a nitric acid plant.

## Acknowledgements

This work was supported by the Ministry of Education, Youth and Sports of the Czech Republic (projects Nos. 6198910016 and MSM 6046137302). We thank to Dr. Zdenek Bastl from J. Heyrovsky Institute of Physical Chemistry ASCR, Prague for XPS analysis.

## References

[1] BAT document, Draft BREF LVIC, 2003.
[2] F. Kapteijn, J.R. Mirasol, J.A. Moulijn, Appl. Catal. B 9 (1996) 25–64.
[3] J. Pérez-Ramírez, F. Kapteijn, G. Mul, X. Xu, J.A. Moulijn, Catal. Today 76 (2002) 55–74.
[4] J. Pérez-Ramírez, F. Kapteijn, A. Brückner, J. Catal. 218 (2003) 234–238.
[5] B.R. Wood, J.A. Reimer, A.T. Bell, M.T. Janicke, K.C. Ott, J. Catal. 224 (2004) 148–155.
[6] A. Wącław, K. Nowińska, W. Schwieger, A. Zielińska, Catal. Today 90 (2004) 21–25.
[7] D. Kaucký, K. Jíša, A. Vondrová, J. Nováková, Z. Sobalík, J. Catal. 242 (2006) 270–277.
[8] L. Kiwi-Minsker, D.A. Bulushev, A. Renken, Catal. Today 91–92 (2004) 165–170.
[9] J.A.Z. Pieterse, S. Booneveld, R.W. van den Brink, Appl. Catal. B 51 (2004) 215–228.
[10] J.A.Z. Pieterse, G. Mul, I. Melian-Cabrera, R.W. van den Brink, Catal. Lett. 99 (2005) 41–44.
[11] J. Oi, A. Obuchi, G.R. Bamwenda, A. Ogata, H. Yagita, S. Kushiyama, K. Mizuno, Appl. Catal. B 12 (1997) 277–286.
[12] S. Suárez, C. Saiz, M. Yates, J.A. Martin, P. Avila, J. Blanco, Appl. Catal. B 55 (2005) 57–64.
[13] S.C. Christoforou, E.A. Efthimiadis, I.A. Vasalos, Catal. Lett. 79 (2002) 137–147.
[14] T.N. Angelidis, V. Tzitzios, Ind. Eng. Chem. Res. 42 (2003) 2996–3000.
[15] Z. Liu, M.D. Amiridis, Y. Chen, J. Phys. Chem. B 109 (2005) 1251–1255.
[16] Z.H. Zhu, H.Y. Zhu, S.B. Wang, G.Q. Lu, Catal. Lett. 91 (2003) 73–81.
[17] Z. Schay, L. Guczi, G. Pal-Borbely, A.V. Ramaswamy, Catal. Today 84 (2003) 165–171.
[18] B.I. Palella, M. Cadoni, A. Frache, H.O. Pastore, R. Pirone, G. Russo, S. Coluccia, L. Marchese, J. Catal. 217 (2003) 100–106.
[19] C.S. Swamy, et al., US Patent 5 472 652 (1995) to Engelhard Corporation.
[20] K.S. Chang, H. Song, Y.S. Park, J.W. Woo, Appl. Catal. A 273 (2004) 223–231.
[21] M.C. Román-Martínez, F. Kapteijn, D. Cazorla-Amorós, J. Pérez-Ramírez, J.A. Moulijn, Appl. Catal. A 225 (2002) 87–100.
[22] J. Pérez-Ramírez, J.M. García-Cortés, F. Kapteijn, M.J. Illán-Gómez, A. Ribera, C. Salinas-Martínez de Lecea, J.A. Moulijn, Appl. Catal. B 25 (2000) 191–203.
[23] J. Pérez-Ramírez, F. Kapteijn, K. Schöffel, J.A. Moulijn, Appl. Catal. B 44 (2003) 117–151.
[24] T.S. Farris, Z. Li, J.N. Armor, T.A. Braymer, US Patent 5 472 677 (1995).
[25] S. Kannan, C.S. Swamy, Catal. Today 53 (1999) 725–737.
[26] J. Pérez-Ramírez, F. Kapteijn, J.A. Moulijn, Catal. Lett. 60 (1999) 133–138.
[27] S. Kannan, Appl. Clay Sci. 13 (1998) 347–362.
[28] S. Kannan, C.S. Swamy, Appl. Catal. B 3 (1994) 109–116.
[29] J. Oi, A. Obuchi, A. Ogata, G.R. Bamwenda, R. Tanaka, T. Hibino, S. Kushiyama, Appl. Catal. B 13 (1997) 197–203.
[30] K.S. Chang, H.-J. Lee, Y.-S. Park, J.-W. Woo, Appl. Catal. A 309 (2006) 129–138.
[31] J.N. Armor, T.A. Braymer, T.S. Farris, Y. Li, F.P. Petrocelli, E.L. Weist, S. Kannan, C.S. Swamy, Appl. Catal. B 7 (1996) 397–406.
[32] J. Pérez-Ramírez, G. Mul, X. Xu, F. Kapteijn, J.A. Moulijn, in: A. Corma, F.V. Melo, S. Mendioroz, J.L.G. Fierro (Eds.), Stud. Surf. Sci. Catal., vol. 130, Elsevier Science, 2000, pp. 1445–1450.
[33] P. Kustrowski, L. Chmielarz, A. Rafalska-Lasocha, B. Dudek, A. Wegrzyn, R. Dziembaj, Przem. Chem. 82 (2003) 732–735.
[34] L. Obalová, K. Jirátová, F. Kovanda, M. Valášková, J. Balabánová, K. Pacultová, J. Mol. Catal. A 248 (2006) 210–219.
[35] L. Obalová, K. Pacultová, J. Balabánová, K. Jirátová, Z. Bastl, M. Valášková, Z. Lacný, F. Kovanda, Catal. Today 119 (2007) 233–238.
[36] L. Obalová, K. Jirátová, F. Kovanda, K. Pacultová, Z. Lacný, Z. Mikulová, Appl. Catal. B 60 (2005) 289–297.
[37] A. Nielsen (Ed.), Ammonia: Catalysis and Manufacture, Springer-Verlag, Berlin, New York, 1995.
[38] M. Haneda, Y. Kintaichi, N. Bion, H. Hamada, Appl. Catal. B 46 (2003) 473–482.
[39] M. Haneda, Y. Kintaichi, H. Hamada, Appl. Catal. B 55 (2005) 169–175.
[40] G. Goula, P. Katzourakis, N. Vakakis, T. Papadam, M. Konsolakis, M. Tikhov, I.V. Yentekakis, Catal. Today 127 (2007) 199–206.
[41] N. Macleod, J. Isaac, R.M. Lambert, J. Catal. 198 (2001) 128–135.
[42] S.M. Park, J.W. Park, H.-P. Ha, H.-S. Han, G. Seo, J. Mol. Catal. A 273 (2007) 64–72.
[43] H. Si-Ahmed, M. Calatayud, C. Minot, E. Lozano Diz, A.E. Lewandowska, M.A. Banares, Catal. Today 126 (2007) 96–102.
[44] M. De, D. Kunzru, Catal. Lett. 102 (2005) 237–246.
[45] M. Kuriyama, H. Tanaka, S. Ito, T. Kubota, T. Miyao, S. Naito, K. Tomishige, K. Kunimori, J. Catal. 252 (2007) 39–48.
[46] N. Iwasa, S. Arai, M. Arai, Catal. Commun. 7 (2006) 839–842.
[47] Y. Yhang, Y. Mou, P. Yu, Y. Yhang, X. Ni, Catal. Commun. 8 (2007) 1621–1624.
[48] A. Kotarba, G. Adamski, Z. Sojka, G.D. Mariadassou, Appl. Surf. Sci. 161 (2000) 105–108.
[49] J. Haber, T. Machej, J. Janas, M. Nattich, Catal. Today 90 (2004) 15–19.
[50] J. Haber, M. Nattich, T. Machej, Appl. Catal. B 77 (2008) 278–283.
[51] C. Ohnishi, K. Asano, S. Iwamoto, K. Chikama, M. Inoue, Catal. Today 120 (2007) 145–150.
[52] K. Asano, Ch. Ohnishi, S. Iwamoto, Y. Shioya, M. Inoue, Appl. Catal. B 78 (2008) 242–249.
[53] F. Zasada, P. Stelmachowski, G. Maniak, J.-F. Paul, A. Kotarba, Z. Sojka, Catal. Lett. 127 (2009) 126–131.
[54] P. Stelmachowski, G. Maniak, A. Kotarba, Z. Sojka, Catal. Commun., doi:10.1016/j.catcom.2008.12.057.
[55] L. Xue, Ch. Zhang, H. He, Y. Teraoka, Catal. Today 126 (2007) 449–455.
[56] H. Cheng, Y. Huang, A. Wang, L. Li, X. Wang, T. Zhang, Appl. Catal. B, doi:10.1016/j.apcatb.2008.12.018.
[57] J.H. Scofield, J. Electron. Spectrosc. Relat. Phenom. 8 (1971) 128.
[58] F. Kovanda, T. Rojka, J. Dobešová, V. Machovič, P. Bezdička, L. Obalová, K. Jirátová, T. Grygar, J. Solid State Chem. 179 (2006) 812–823.
[59] B. Lamontagne, F. Semond, D. Roy, Surf. Sci. 327 (1995) 371–378.
[60] S. Ribet, D. Tichit, B. Coq, B. Ducourant, F. Morato, J. Solid State Chem. 142 (1999) 382–392.

[61] P. Arnoldy, J.A. Moulijn, J. Catal. 93 (1985) 38–54.
[62] M. Ferrandon, J. Carnö, S. Järås, E. Björnbom, Appl. Catal. A 180 (1999) 141–151.
[63] G. Fierro, M.L. Jacono, M. Inversi, R. Dragone, G. Ferraris, Appl. Catal. B 30 (2001) 173–185.
[64] A. Bielanski, J. Haber, Oxygen in Catalysis, Marcel Dekker, Inc., New York, 1991.
[65] A.L. Yakovlev, G.M. Zhidomirov, R.A. van Santen, Catal. Lett. 75 (2001) 45–48.
[66] L. Obalová, V. Fíla, Appl. Catal. B 70 (2007) 353–359.
[67] H. Dandl, G. Emig, Appl. Catal. A 168 (1998) 261–268.
[68] J.W. Niemantsverdriet, Spectroscopy in Catalysis, 2nd ed., Wiley-VCH, 2000.
[69] S. Alini, F. Basile, A. Bologna, T. Montanari, A. Vaccari, in: E. E. Gaigneaux (Ed.), Studies in Surface Science and Catalysis, vol. 143, Elsevier Science, 2000 pp. 131–139.
[70] P.J. Smeets, B.F. Sels, R.M. van Teeffelen, H. Leeman, E.J.M. Hensen, R.A. Schoonheydt, J. Catal. 256 (2008) 183–191.
[71] J.A.Z. Pieterse, G.D. Pirngruber, J.A. van Bokhoven, S. Booneveld, Appl. Catal. B 71 (2007) 16–22.
[72] D.A. Bulushev, P.M. Prechtl, A. Renken, L. Kiwi-Minsker, Ind. Eng. Chem. Res. 46 (2007) 4178–4185.
[73] Smeets, Q. Shen, L. Li, J. Li, H. Tian, Z. Hao, J. Hazard. Mater., doi:10.1016/j.jhazmat.2008.07.104.
[74] G.E. Marnellos, E.A. Efthimiadis, I.A. Vasalos, Appl. Catal. B 46 (2003) 523–539.
[75] D. Berthomieu, N. Jardillier, G. Delahay, B. Coq, A. Goursot, Catal. Today 110 (2005) 294–302.